American Journal of Engineering Research (AJER)
e-ISSN : 2320-0847 p-ISSN : 2320-0936
Volume-02, Issue-07, pp-49-61
www.ajer.org

Research Paper Open Access

Natural convection of the localized heat sources of T-shaped nanofluid-filled enclosures

M. A. Mansour, A. Y. Bakier, M. A. Y. Bakier
Department of Mathematics, Faculty of Sciences, Assiut University, Assiut, Egypt

Abstract: - Natural convection fluid flow and heat transfer inside T-shaped enclosures filled with Cu-Water nanofluid has been investigated numerically using finite difference method. A parametric study was conducted and effects of pertinent parameters such as Rayleigh number, the aspect ratio of the T-shaped enclosure, and the volume fraction of the Cu nanoparticles on the flow and temperature fields and the rate of heat transfer inside the enclosure were investigated. It was found from the obtained results that the mean Nusselt number increased with increase in Rayleigh number and volume fraction of Cu nanoparticles regardless aspect ratio of the enclosure. Moreover the obtained results showed that the rate of heat transfer increased with decreasing the aspect ratio of the cavity. Also it was found that the rate of heat transfer increased with increase in nanoparticles volume fraction. Also at low Rayleigh numbers, the effect of Cu nanoparticles on enhancement of heat transfer for narrow enclosures was more than that for wide enclosures.

Keywords: - *Natural convection, nanofluid, T-shaped cavity, Nusselt number, Rayleigh number.*

I. INTRODUCTION

Nanofluid, which is a mixture of nano-sized particles (nanoparticles) suspended in a base fluid, is used to enhance the rate of heat transfer via its higher thermal conductivity compared to the base fluid. Mahmoodi [1] investigated numerically free convection of Cu-water nanofluid in L-shaped and C-shaped cavities. He found that effect of presence of nanoparticles on heat transfer enhancement is more apparent for narrow L-shaped and C-shaped cavities.

Many researchers have simulated the heat removal mechanism by means of natural convection in enclosures heated from below [3, 4]. More recently, Cheikh et al. [5] studied natural convection in a square enclosure heated from below and cooled from above for a variety of thermal boundary conditions at the top and sidewalls. They carried out their simulation for two different lengths of the heat source and various Rayleigh numbers. They argued that the maximum temperature of the heat source did not change significantly for the diffusion dominated cases whereas decreased rather rapidly with Rayleigh number for convection dominated regimes.

In most natural convection studies, the base fluid in the enclosure has a low thermal conductivity, which limits the heat transfer enhancement. However, the continuing miniaturization of electronic devices requires further heat transfer improvements from an energy saving viewpoint. An innovative technique, which uses a mixture of nanoparticles and the base fluid was first introduced by Choi [6] in order to develop advanced heat transfer fluids with substantially higher conductivities. The resulting mixture of the base fluid and nanoparticles having unique physical and chemical properties is referred to as a nanofluid. It is expected that the presence of the nanoparticles in the nanofluid increases the thermal conductivity and therefore substantially enhances the heat transfer characteristics of the nanofluid.

Eastman et al. [7], Xie et al. [8] showed that higher thermal conductivity can be achieved in thermal systems utilising nanofluids. In recent years thermophysical properties of nanofluids have been investigated by many researchers [9-14]. Investigation of different applications of nanofluids can be found in literature such as forced convection of nanofluids (Namburu et al. [16], Santra et al. [17] and Strandberg and Das [18]), boiling heat transfer of nanofluids (Das et al. [19]) and mixed convection of nanofluids (Akbarinia and Behzadmehr

[20], Akbari et al. [21], Ghaffari et al. [22], Mahmoodi [23] and Arefmanesh and Mahmoodi [24]).There are a number of recent studies on free convection inside cavities containing nanofluid. Khanafer et al. [25] investigated numerically the problem of free convection of nanofluid in rectangular cavities with cold right wall, hot left wall and insulated horizontal walls. They found that the rate of heat transfer increased with increase in nanoparticles volume fraction. Since the free convection heat transfer of nanofluids in the thermal engineering applications will be extending the existing knowledge, the authors are motivated by interest in investigation of the effects of a nanofluid in the laminar free convection heat transfer in T-shaped enclosures. The most convenient application of T-shaped enclosures can be cooling of some electronic parts in the manufactures. Using the nanofluids the efficiency of the cooling can be enhanced. In the present study the governing equations in terms of primitive variables in Cartesian coordinate system are discretized using the finite difference method. The effects of aspect ratio of enclosure, nanoparticles volume fraction and Rayleigh number on the flow and temperature fields and heat transfer characteristics are discussed.

In the present paper natural convection fluid flow and heat transfer of Cu-water nanofluid inside T-shaped enclosure was studied numerically and the effects of the Rayleigh number, aspect ratio of enclosure and volume fraction of the nanoparticles on flow pattern, temperature field and rate of heat transfer were investigated.

II. MATHEMATICAL MODELING

$$\frac{\partial u}{\partial x}+\frac{\partial v}{\partial y}=0 \tag{1}$$

$$u\frac{\partial u}{\partial x}+v\frac{\partial u}{\partial y}=-\frac{1}{\rho_{nf}}\frac{\partial p}{\partial x}+\frac{\mu_{nf}}{\rho_{nf}}\left(\frac{\partial^2 u}{\partial x^2}+\frac{\partial^2 u}{\partial y^2}\right) \tag{2}$$

$$u\frac{\partial v}{\partial x}+v\frac{\partial v}{\partial y}=-\frac{1}{\rho_{nf}}\frac{\partial p}{\partial y}+\frac{\mu_{nf}}{\rho_{nf}}\left(\frac{\partial^2 v}{\partial x^2}+\frac{\partial^2 v}{\partial y^2}\right)+\frac{(\rho\beta)_{nf}}{\rho_{nf}}g(T-T_C) \tag{3}$$

$$u\frac{\partial T}{\partial x}+v\frac{\partial T}{\partial y}=\alpha_{nf}\left(\frac{\partial^2 T}{\partial x^2}+\frac{\partial^2 T}{\partial y^2}\right) \tag{4}$$

$$\rho_{nf}=(1-\varphi)\rho_f+\varphi\rho_s \tag{5}$$

$$(\rho c_p)_{nf}=(1-\varphi)(\rho c_p)_f+\varphi(\rho c_p)_s \tag{6}$$

$$(\rho\beta)_{nf}=(1-\varphi)(\rho\beta)_f+\varphi(\rho\beta)_s \tag{7}$$

$$\alpha_{nf}=\frac{k_{nf}}{(\rho c_p)_{nf}} \tag{8}$$

$$\beta_{nf}=\frac{(1-\varphi)(\rho\beta)_f+\varphi(\rho\beta)_s}{(1-\varphi)\rho_f+\varphi\rho_s} \tag{9}$$

$$\mu_{eff}=\frac{\mu_f}{(1-\varphi)^{2.5}} \tag{10}$$

$$\frac{k_{nf}}{k_f}=\frac{(k_s+2k_f)-2\varphi(k_f-k_s)}{(k_s+2k_f)+\varphi(k_f-k_s)} \tag{11}$$

$$X=\frac{x}{H},\ Y=\frac{y}{H},\ U=\frac{uH}{\alpha_f},\ V=\frac{vH}{\alpha_f}\ P=\frac{pH^2}{\rho_{nf}\alpha_f^2},\quad \theta=\frac{T-T_C}{T_H-T_C} \tag{12}$$

$$\frac{\partial U}{\partial X}+\frac{\partial V}{\partial Y}=0 \tag{13}$$

$$U\frac{\partial U}{\partial X}+V\frac{\partial U}{\partial Y}=-\frac{1}{\rho_{nf}}\frac{\partial P}{\partial X}+\frac{\mu_{nf}}{\rho_{nf}\alpha_f}\left(\frac{\partial^2 U}{\partial X^2}+\frac{\partial^2 U}{\partial Y^2}\right) \tag{14}$$

$$U\frac{\partial V}{\partial X}+V\frac{\partial V}{\partial Y}=-\frac{1}{\rho_{nf}}\frac{\partial P}{\partial Y}+\frac{\mu_{nf}}{\rho_{nf}\alpha_f}\left(\frac{\partial^2 V}{\partial X^2}+\frac{\partial^2 V}{\partial Y^2}\right)+\frac{(\rho\beta)_{nf}}{\rho_{nf}\beta_f}Ra\,\mathrm{Pr}\,\theta \tag{15}$$

$$U\frac{\partial\theta}{\partial X}+V\frac{\partial\theta}{\partial Y}=\frac{\alpha_{nf}}{\alpha_f}\left(\frac{\partial^2\theta}{\partial X^2}+\frac{\partial^2\theta}{\partial Y^2}\right) \tag{16}$$

$$Ra=\frac{g\beta_f(T_h-T_C)H^3}{\alpha_f\nu_f},\quad \Pr=\frac{\nu_f}{\alpha_f} \tag{17}$$

$$\begin{cases} on\ walls: \begin{cases} ab, cd, gh: U=V=0, \partial\theta/\partial y=0 \\ fe: \begin{cases} U=V=0, \partial\theta/\partial y=1, D-0.5*B\le X\le D+0.5*B \\ U=V=0, \partial\theta/\partial y=0, Otherwise \end{cases} \end{cases} \\ on\ walls\ ah, bc: U=V=0, \theta=0 \\ on\ walls\ de, fg: \ U=V=0, \partial\theta/\partial x=0 \end{cases} \tag{18}$$

$$Nu_{local}=\frac{hH}{k_f} \tag{19}$$

$$h=\frac{q_w}{T_h-T_C} \tag{20}$$

$$k_{nf}=-\frac{q_w}{\partial T/\partial Y}\ on\ wall\ \ fe \tag{21}$$

$$Nu_l=-\left(\frac{k_{nf}}{k_f}\right)\frac{\partial\theta}{\partial Y}\ onwall\ fe \tag{22}$$

$$Nu_m=\left(\int_{D-0.5*B}^{D+0.5*B} Nu_l\,dX\Big|_{Y=1}\right) \tag{23}$$

III. NUMERICAL METHOD AND VALIDATION

In this investigation, the finite difference method (Mansour et al. [26]) was employed to solve the governing equations with the boundary conditions. Central difference quotients were used to approximate the second derivatives in both the-XandY-directions. Then, the obtained discretized equations are solved using a Gauss-Seidel iteration technique (Grosan et al.[27]; Singh and Venkateshan [28]). The solution procedure is iterated until the following convergence criterion is satisfied:

$$\sum_{i,j}\left|\chi_{i,j}^{new}-\chi_{i,j}^{old}\right|\le 10^{-7}$$

where χ is the general dependent variable. The numerical method was implemented in FORTRAN software. In order to verify the accuracy of present method, the obtained results in special cases are compared with the results obtained by Walker and Homsy [29], Gross et al.[30], Manole and Lage [31]. Table 2 shows a good agreement was found between the present results and the results obtained by the previous works. These favorable comparisons lend confidence in the numerical results to be reported subsequently.

The finite difference method uses four sets of grids: 36×36, 66×66, 96×96, and 126×126 as shown in Table 3. There is a good agreement was found between 66 × 66 and 126× 126 grids, so the numerical computations were carried out for 66 × 66 and 126× 126 grid nodal points.

IV. RESULTS AND DISCUSSION

The results are presented in terms of streamlines, isotherms, average Nusselt number and local Nusselt number. Fig. 2 illustrates effect of increase in AR on flow pattern and temperature distribution inside the enclosures filled with pure fluid (ϕ = 0) at *Ra* = 10^5. As can be seen from the streamlines in the figure, for *AR* = 0.3 the fluid is heated by the sources and expands as it moves downward. Then the fluid is cooled by the cold ribs and compressed as it moves upward. Hence, there is a symmetrical behavior for the stream lines. The isotherms for this aspect ratio are condensed adjacent to the top of the cavity, because the top wall has a

maximum effect in heating the fluid. Moreover as the T-shaped enclosure becomes narrower the local Rayleigh number and buoyancy force in the top region of the cavity. The corresponded isotherms show that for *AR*= 0.9 thermal stratification occurs in the gaps over the cold rib. Also it must be noted that when the aspect ratio of the cavity increases, the isotherms becomes more evenly distributed on the top of the cold rib. From the observed result maximum and minimum limits are found for developing the Rayleigh-Bénard cells in the gap between the source and the cold rib. Also it can be considered that the walls *cd* and *gh* work as temperature pumps in the cavity, that is for *AR*<0.6, where its effect is clear.

Fig. 3 shows the streamlines and isotherms inside the T – shape enclosure filled with pure fluid at *AR*=0.3, *D*=.5, $Ra=10^5$, and for various lengths of heat source. There is no great change among the contours. Only one thing can be noticed, as B is small, as heat transfer is obvious.

Fig. 4 shows streamlines and isotherms inside the T – shape enclosure filled with pure fluid (ϕ =0.0) at $Ra=10^5$, *AR*=0.3, *B*=1/3 and for different heat source locations. The symmetric behavior decays as the source moving away from the middle.

Fig. 5 shows streamlines and isotherms inside the T– shape enclosure filled with nanofluid (ϕ =0.1) at $Ra=10^5$, *B*=1/3, *D*=.5 for different aspect ratios of enclosure. There isn't great change from pure case.

Fig. 6 shows streamlines and isotherms at $Ra=10^5$, *AR*=0.3 and for different heat source lengths. It is clear that the heat transfer is very week and takes its huge value at B=0.6.

Fig. 7 shows streamlines and isotherms inside the T – shape enclosure filled with nanofluid at $Ra=10^5$, *AR*=0.3, *D*=.5, *B*=1/3 and for various values of solid volume fraction. The effect of (ϕ) is week as seems from contours.

Fig. 8 shows streamlines and isotherms inside the T – shape enclosure filled with nanofluid at $Ra=10^5$, *AR*=0.3, D=.5, B=1/3 and for various nonoparticles. As seems from contours, the various nanofluids don't have great different from each others.

Fig.9. presented the profiles of (a) θ_s -X curves for different solid volume fractions, it's clear that the source temperature decreases as the solid volume fraction increases. Also, the profiles are symmetric around the middle of the top wall where the curves reach to its unique maximum values, while in the ends there are its two minimum points. Fig. 9(b) shows the variations of local Nusselt number along the heat source for different solid volume fractions. It is obvious that the curves inverse the previous curves in (a).

Fig. 10 shows the variation of the local Nusselt number along the heat source for different heat source lengths. It is shown that the profiles are symmetric. Generally, the heat transfer decreases as the heat source length increases, and the curve becomes more flat.

Fig. 11 shows the profiles of Nu_m-ϕ for various heat source lengths, it confirms that the average Nusselt number increases as the solid volume fraction increases. But it decreases as *B* increases.

Fig. 12 shows the profiles of Nu_m-ϕ for various aspect ratios, *AR*, it can be noticed that the average Nusselt number decreases as *AR* increases. It is can verified that there is no effect for *AR* in pure case. However, the effect of the aspect ratio increases and can be more obviousness as the solid volume fraction increases.

Fig. 13 shows the profiles of Nu_m-ϕ for various Rayleigh number, for $Ra<5x10^5$ the rate is nearly congruent, often the average Nusselt number increases as Raleigh number increases.

Fig. 14 shows variation of average Nusselt number with heat source location at various aspect ratios where *B*=1/3, $Ra=10^5$ and ϕ =0.1. it can verified from the curves that the effect of the location of heat source increases greatly, as the aspect ratio increases. So there is a huge difference at *AR*=0.9, while the change tend to be zero at *AR*=.3.

Fig.15 presents the effects of the length of heat source on its average Nusselt number for different aspect ratios. As stated, the heat transfer decreases as the heat source length increases. The difference between the end-point and the start-point decreases as *AR* increases.

Fig. 16 shows the profile of local Nusselt number along the heat source for different types of nanofluids. Profiles are obtained for all nanofluids with the lowest Nusselt number for the middle of the heat source. It is clear that the smallest values for Nu_s are on the curve of pure water; conversely, the biggest values are on curve of TiO_2. Table 1 shows that TiO_2 has the lowest

value of thermal conductivity compared to other nanoparticles, hence, it has the lowest values of Nusselt number. Cu and Ag, on the other hand, have the highest values. In addition, the thermal conductivity of Al_2O_3 is approximately one tenth of Cu and Ag (Table 1), thus, the Nusselt number for Al_2O_3 is lower than that for Cu and Ag. Fig. 23 presents the variation of average Nusselt number with solid volume fraction.

Table 4 shows that changing nanotypes does not affect both Nu_m and maximum temp., but that is not for

stream function values. Cu and Ag decrease ψ_{max} values. On the contrary, the other types are. Rayleigh number has not significant effect on Nu_m and θ_{max} but it enhances the stream values. Table 5 displays the effect of aspect ratio which supplies both ψ_{max} and θ_{max}, but it decreases the average Nusselt nuber values.

V. CONCLUSION

Natural convection in a partially heated enclosure from bottom and top, filled with different types of nanofluids has been numerically investigated by finite difference method. The effects on the enclosure cooling performance of Rayleigh number, solid volume fraction, heat source length and location and the type of nanofluid are studied.The increase of Rayleigh numbers strengthens the natural convection flows which results in the reduction of heat source temperature. Also the increase of solid volume fraction of nanoparticles causes the heat source maximum temperature to decrease particularly at low Rayleigh numbers where conduction is the main heat transfer mechanism. The increase of heat source length increases the heat transfer to the nanofluid and therefore, increases the surface temperature of the heat source and the strength of natural convection circulating cells within the enclosure. As the heat source moves from the left wall towards the middle of the bottom wall of the enclosure, at low Rayleigh numbers, the heat source maximum temperature continuously increases. At high Rayleigh number, minimum rate of heat transfer occurs from top wall and its minimum occurs from the bottom wall while at low Rayleigh number similar rates heat transfer from top and bottom walls are observed.
As the T-shaped enclosure becomes narrower, the rate of heat transfer increases. Also as the Rayleigh number increases, the rate of heat transfer increases for a constant AR.

REFERENCES

[1] Mostafa Mahmoodi, Seyed Mohammad Hashemi, Numerical study of natural convection of a nanofluid in C-shaped enclosures, International Journal of Thermal Sciences 55 (2012) 76-89.
[2] I. Sezai, A.A. Mohamad, Natural convection from a discrete heat source on the bottom of a horizontal enclosure, Int. J. Heat Mass Transf. 43 (2000) 2257–2266.
[3] M. Corcione, Effects of the thermal boundary conditions at the sidewalls upon natural convection in rectangular enclosures heated from bellow and cooled from above, Int. J. Therm. Sci. 42 (2003) 199–208.
[4] B. Calgagni, F. Marsili, M. Paroncini, Natural convective heat transfer in square enclosures heated from below, Appl. Therm. Eng. 25 (2005) 2522–2531.
[5] N.B. Cheikh, B.B. Beya, T. Lili, Influence of thermal boundary conditions on natural convection in a square enclosure partially heated from below, Int. Comm. Heat Mass Transf. 34 (2007) 369–379.
[6] S.U.S. Choi, Enhancing thermal conductivity of fluids with nanoparticles. ASME Fluids Eng Div 1995, 231, 99–105.
[7] J.A. Eastman, S.U.S. Choi, S. Li, W. Yu, L.J. Thompson, Anomalously increased effective thermal conductivities of ethylene glycol-based nanofluids containing copper nanoparticles, Appl. Phys. Lett. 78 (6) (2001) 718–720.
[8] H.Q. Xie, H. Lee, W. Youn, M. Choi, Nanofluids containing multiwalled carbon nanotubes and their enhanced thermal conductivities, J. Appl. Phys. 94 (8) (2003) 4967–4971.
[9] S. Jana, A. Salehi-Khojin, W.H. Zhong, Enhancement of fluid thermal conductivity by the addition of single and hybrid nano-additives, Thermochimica Acta 462 (1–2) (2007) 45–55.
[10] S.M. Aminossadati, B. Ghasemi, Natural convection cooling of a localised heat source at the bottom of a nanofluid-filled enclosure, European Journal of Mechanics B/Fluids 28 (2009) 630–640.
[11] H.U. Kang, S.H. Kim, J.M. Oh, Estimation of thermal conductivity of nanofluid using experimental effective particle volume, Exp. Heat Transfer 19 (2006) 181-191.
[12] V. Velagapudi, R.K. Konijeti, C.S.K. Aduru, Empirical correlation to predict thermophysical and heat transfer characteristics of nanofluids, Thermal Sci. 12 (2008) 27-37.
[13] C. Murugesan, S. Sivan, Limits for thermal conductivity of nanofluids, Thermal Sci. 14 (2010) 65-71.
[14] A.K. Nayak, R.K. Singh, P.P. Kulkarni, Measurement of volumetric thermal expansion coefficient of various nanofluids, Tech. Phys. Lett. 36 (2010) 696-698.
[15] M.M. Papari, F. Yousefi, J. Moghadasi, H. Karimi, A. Campo, Modeling thermal conductivity augmentation of nanofluids using diffusion neural networks, Int. J. Thermal Sci. 50 (2011) 44-52.
[16] P.K. Namburu, D.K. Das, K.M. Tanguturi, R.S. Vajjha, Numerical study of turbulent flow and heat transfer characteristics of nanofluids considering variable properties, Int. J. Thermal Sci. 48 (2009) 290-302.
[17] A.K. Santra, S. Sen, N. Chakraborty, Study of heat transfer due to laminar flow of copperewater nanofluid through two isothermally heated parallel plates, Int. J. Thermal Sci. 48 (2009) 391-400.
[18] R. Strandberg, D.K. Das, Finned tube performance evaluation with nanofluids and conventional heat transfer fluids, Int. J. Thermal Sci. 49 (2010) 580-588.

[19] S.K. Das, N. Putra, W. Roetzel, Pool boiling characterization of nano-fluids, Int. J. Heat Mass Tranf. 46 (2003) 851-862.
[20] A. Akbarinia, A. Behzadmehr, Numerical study of laminar mixed convection of a nanofluid in horizontal curved tubes, Appl. Thermal Eng. 27 (2007) 1327-1337.
[21] M. Akbari, A. Behzadmehr, F. Shahraki, Fully developed mixed convection in horizontal and inclined tubes with uniform heat flux using nanofluid, Int. J. Heat Fluid Flow 29 (2008) 545-556.
[22] O. Ghaffari, A. Behzadmehr, H. Ajam, Turbulent mixed convection of a nanofluid in a horizontal curved tube using a two-phase approach, Int. Comm. Heat Mass Trans. 37 (2010) 1551-1558.
[23] M. Mahmoodi, Mixed convection inside nanofluid filled rectangular enclosures with moving bottom wall, Thermal Sci. 15 (2011) 889-903.
[24] A. Arefmanesh, M. Mahmoodi, Effects of uncertainties of viscosity models for Al2O3ewater nanofluid on mixed convection numerical simulations, Int. J. Thermal Sci. 50 (2011) 1706-1719.
[25] K. Khanafer, K. Vafai, M. Lightstone, Buoyancy-driven heat transfer enhancement in a two-dimensional enclosure utilizing nanofluid, Int. J. Heat Mass Tran. 46 (2003) 3639-3653.
[26] M.A.Mansour, A.J. Chamkha, R.A.Mohamed , M.M.Abd El-Aziz , S.E.Ahmed, MHD natural convection in an inclined cavity filled with a fluid saturated porous medium with heat source in the solid phase. Nonlinear Anal. 15(2010)55–70.
[27] T.Grosan , C.Revnic, I.Pop, D.B.Ingham, Magnetic field and internal heat generation effects on the freeconvection in a rectangular cavity filled with a porous medium. Int. J. Heat Mass Transf. 52(2009)1525–1533.
[28] B.V.Ratish Kumar, P.V.S.N.Murthy, P.Singh, Free convection heat transfer from an isothermal wavy surface in a porous enclosure. Int. J. Numer. Meth. Fluids 28(1998)633–661.
[29] K.L.Walker, G.M.Homsy, Convection in a porous cavity. J. Fluid Mech. 87(1978)449–474.
[30] R.J.Gross , M.R.Bear , C.E.Hickox, The application of flux-corrected transport (FCT) to high Rayleigh number natural convection in a porous medium. In: Proceedings of 8th International Heat Transfer Conference, San Francisco, CA, USA, (1986).
[31] D.M.Manole, J.L.Lage, Numerical benchmark results for natural convection in a porous medium cavity. In:Proceedings of the ASME Conference on Heat and Mass Transfer in Porous Media, HTD, 216 (1992) 55–60.
[32] M.Haajizadeh , A.F.Ozguc and C.L.Tien, Natural convection in a vertical porous enclosure with internal heat generation, *Int. J. Heat Mass Transfer*, 27(1984)1893–190.

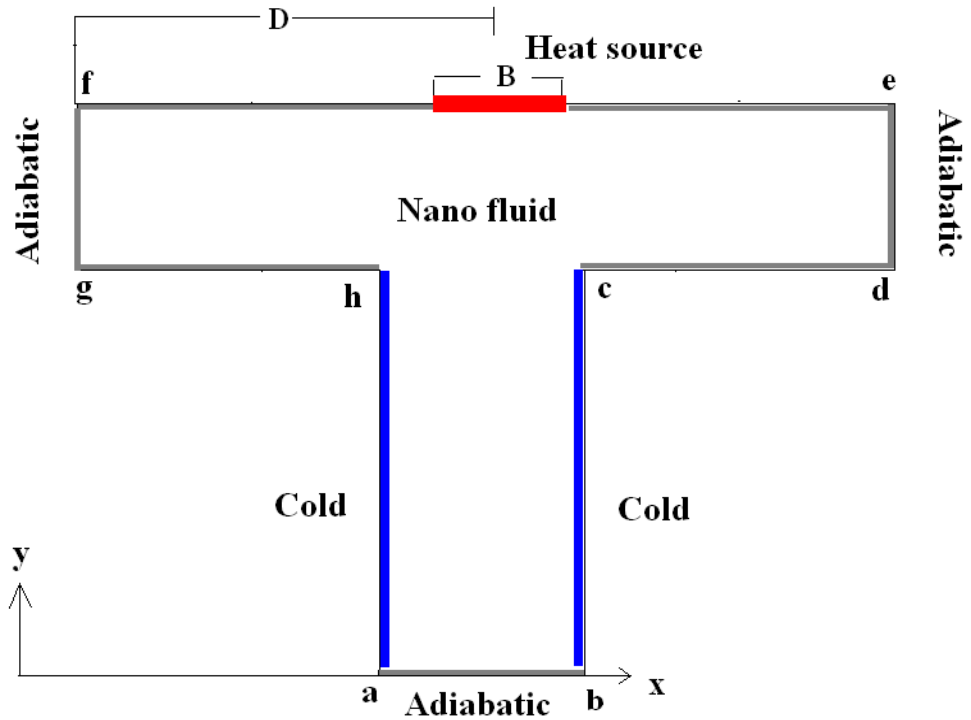

Fig. 1 Physical model of the prblem.

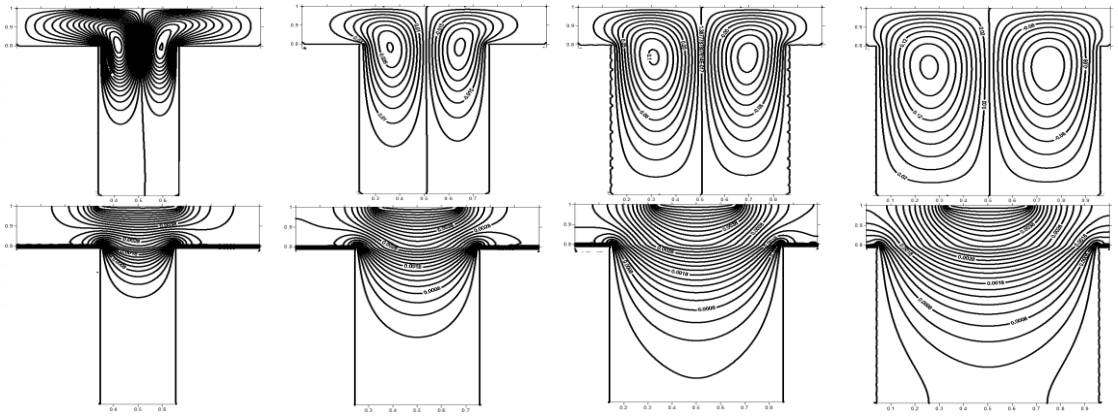

(a) (b) (c) (d)

Fig. 2 Streamlines (top) and isotherms (down) inside the T – shape enclosure filled with pure fluid (ϕ =0.0) at Ra=10^5, B=1/3, D=.5, (a) AR=.3, (b)AR=.5, (c)AR=.7, (d)AR=.9

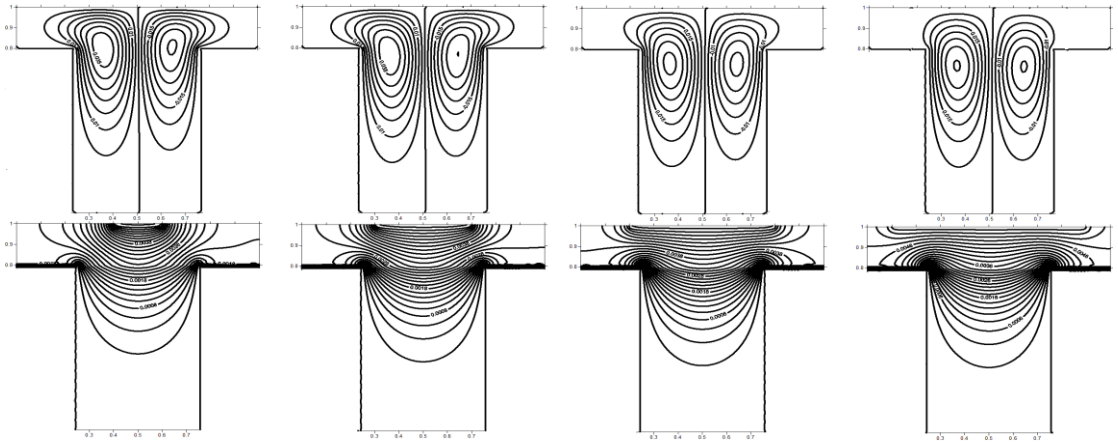

(a) (b) (c) (d)

Fig. 3 Streamlines (top) and isotherms (down) inside the T – shape enclosure filled with pure fluid (ϕ =0.0) at Ra=10^5, AR=0.5, D=.5, (a) B=.2, (b) B=.4, (c)B=.6, (d)B=.8

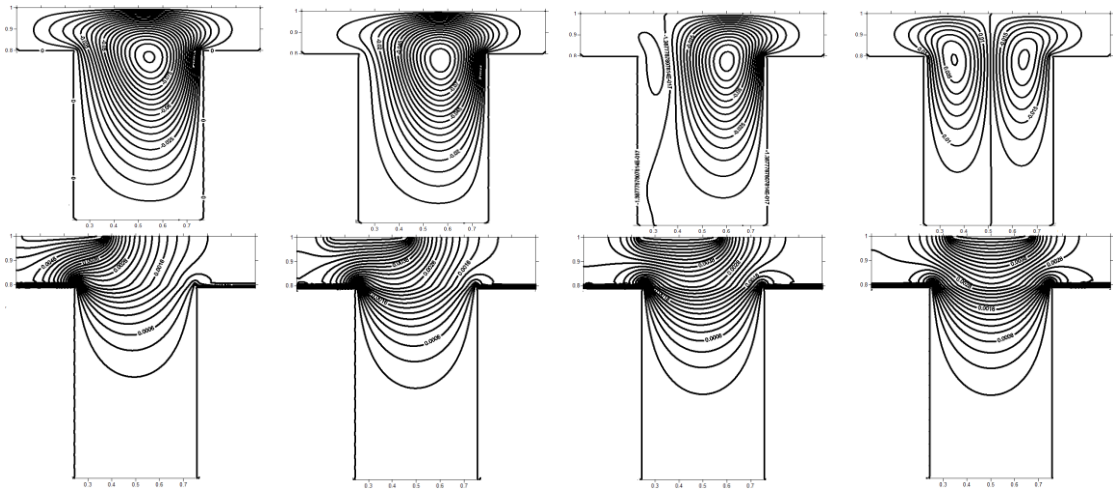

(a) (b) (c) (d)

Fig. 4 Streamlines (top) and isotherms (down) inside the T – shape enclosure filled with pure fluid (ϕ =0.0) at AR=0.5, Ra=10^5,B=1/3.,(a) D=.2, (b) D=.3, (c) D=.4, (d) D=.5

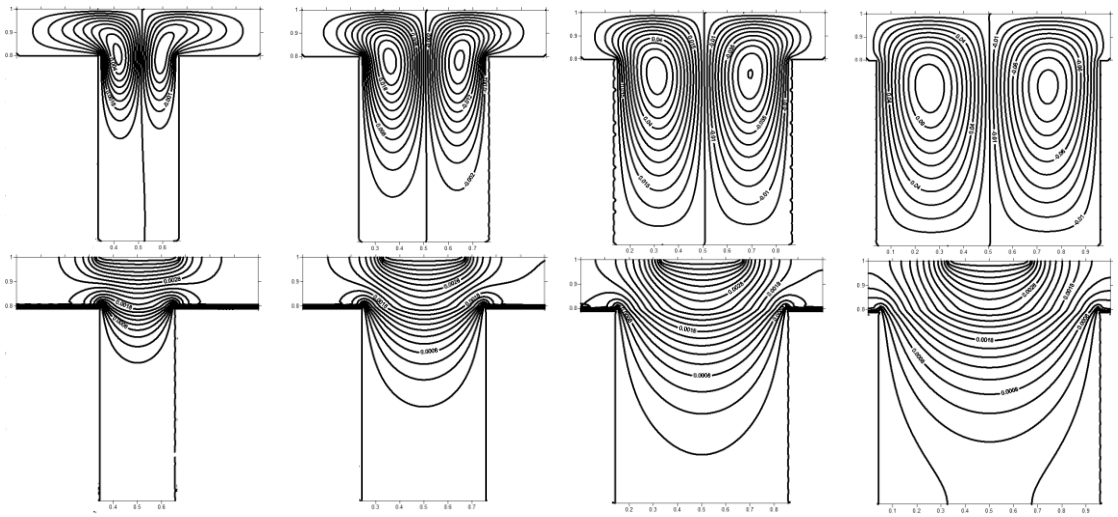

(a) (b) (c) (d)

Fig. 5 Streamlines (top) and isotherms (down) inside the T – shape enclosure filled with nanofluid (ϕ =0.1) at Ra=10^5, B=1/3, D=.5, (a) AR=.3, (b) AR=.5, (c) AR=.7, (d) AR=.9.

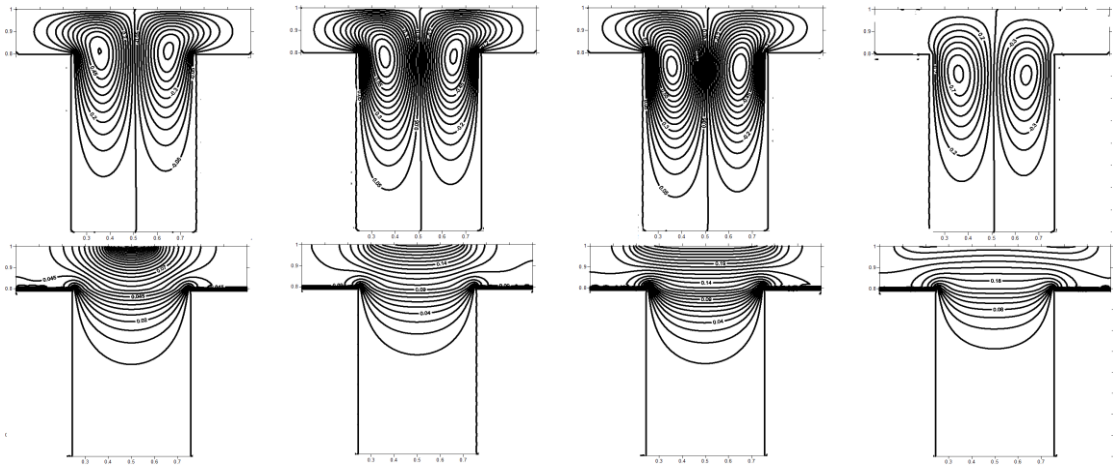

(a) (b) (c) (d)

Fig. 6 Streamlines (top) and isotherms (down) inside the T – shape enclosure filled with nanofluid (ϕ =0.1) at Ra=10^5, AR=0.5, D=.5, (a) B=0.2, (b) B=0.4, (c) B=0.6, (d) B=0.8.

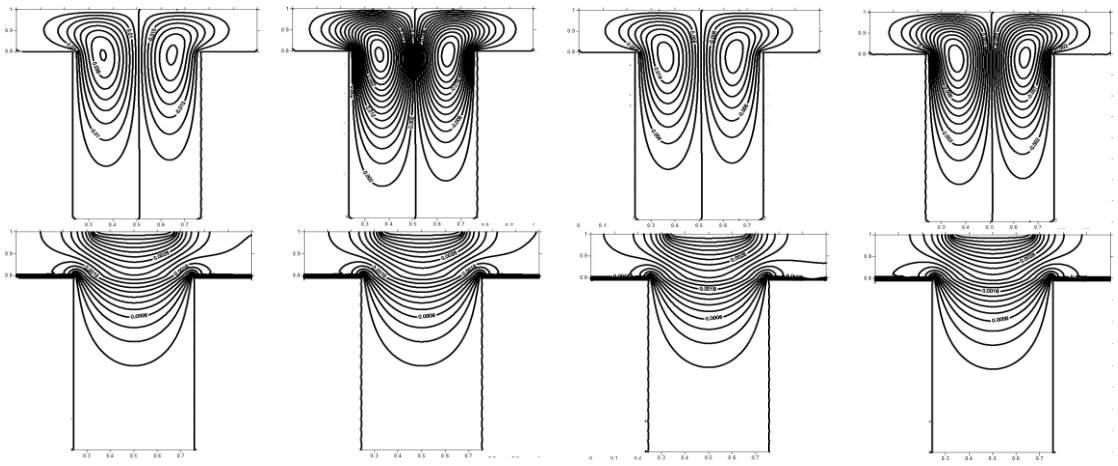

(a) (b) (c) (d)

Fig. 7 Streamlines (top) and isotherms (down) inside the T – shape enclosure filled with nanofluid at Ra=10^5, AR=0.5, D=.5, B=1/3., (a) ϕ =0.0, (b) ϕ =.05, (c) ϕ =0.1, (d) ϕ =0.2

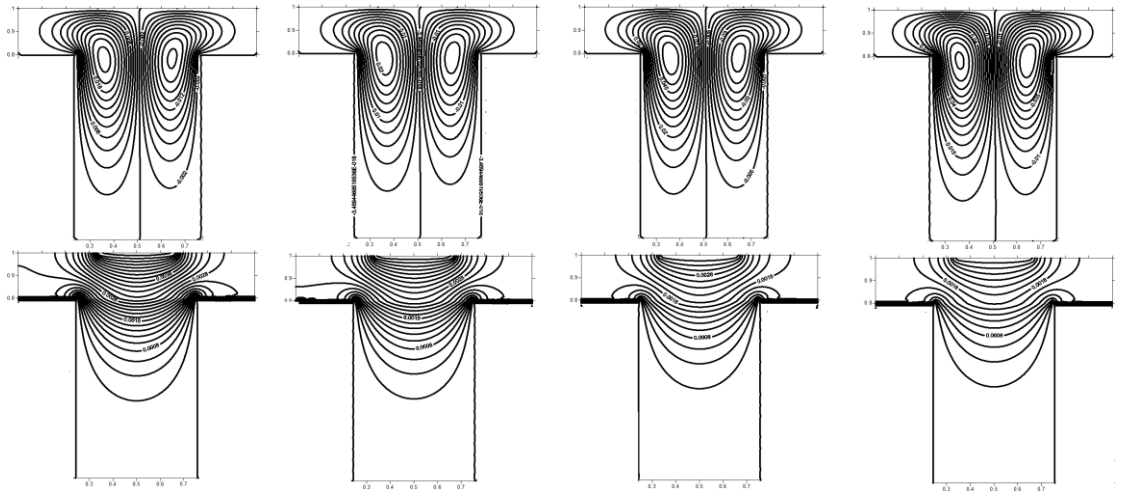

(a) (b) (c) (d)

Fig 8. Streamlines (top) and isotherms (down) inside the T – shape enclosure filled with nanofluid at $Ra=10^5$, AR=0.5, D=.5, B=1/3., ϕ =0.1 ,(a) Cu-water,(b) Ag-Water,(c) Al_2O_3-Water,(d) Ti O_2-Wter

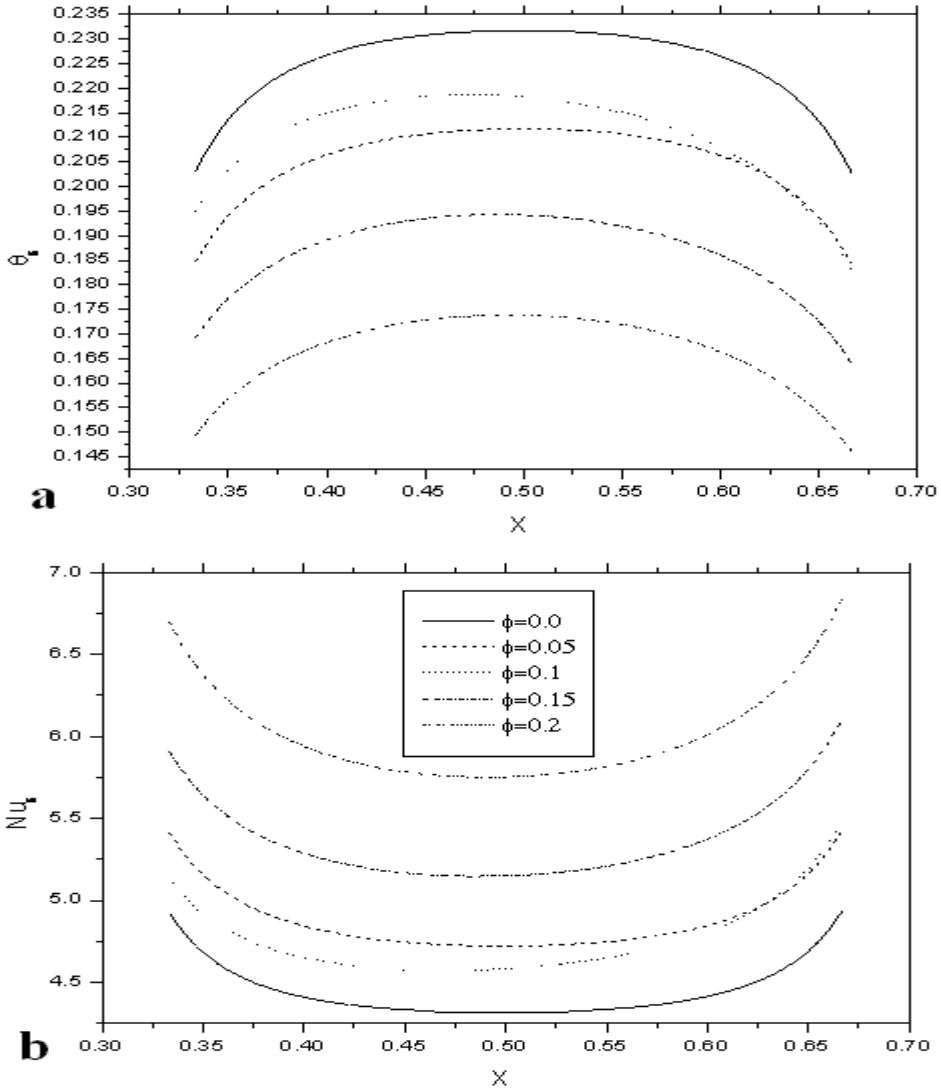

Fig.9. a) Profile of source temperature along the heat source for various solid volume fraction, b) Profile of local Nusselt number along the heat source for various solid volume fraction (Cu-Water, D=0.5, $Ra=10^5$, B=1/3 and AR=0.5)

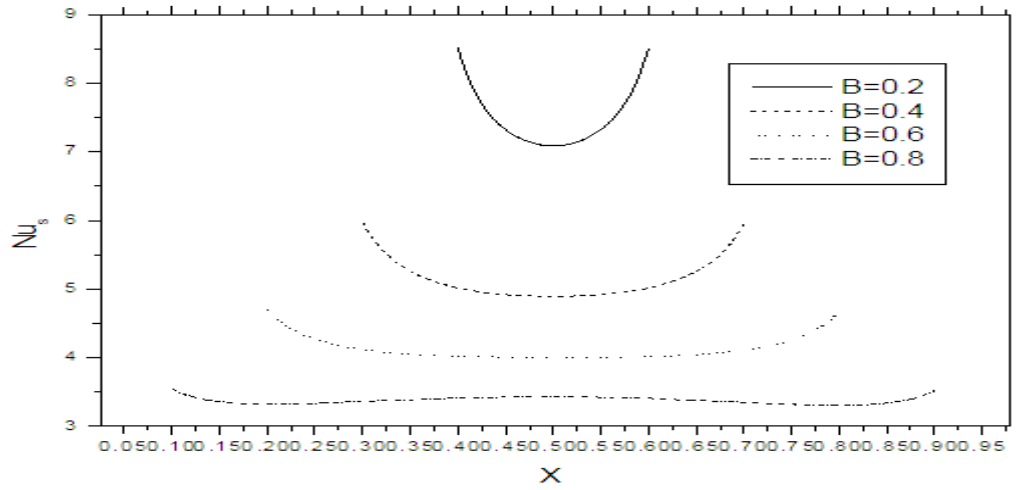

Fig.10. Variation of local Nusselt number along the heat source at the top for various heat source lengths (Cu-Water, D=0.5, Ra=10^5 and AR=0.5).

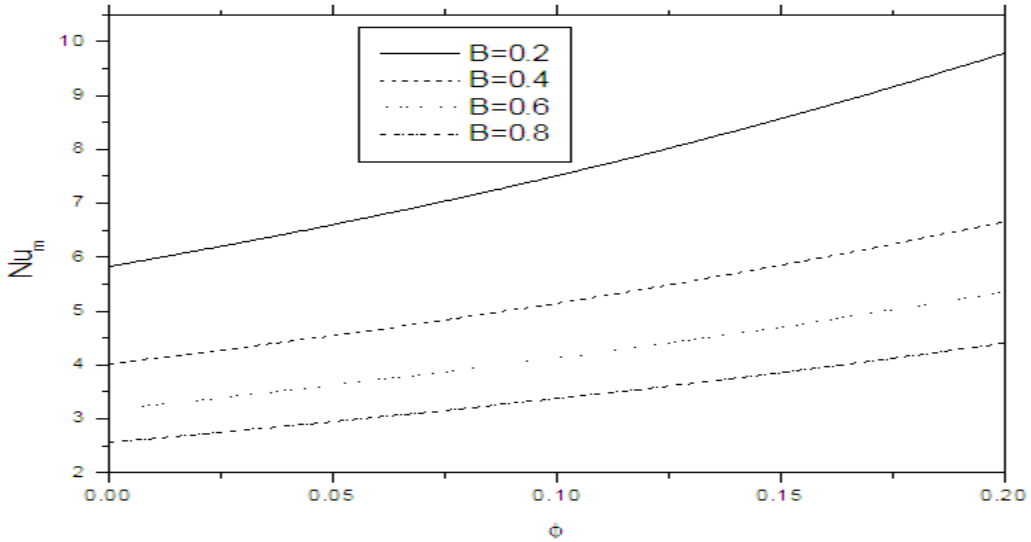

Fig.11. Variation of average Nusselt number with solid volume fraction at various heat source lengths (Cu-Water, D=0.5, Ra=10^5 and AR=0.5).

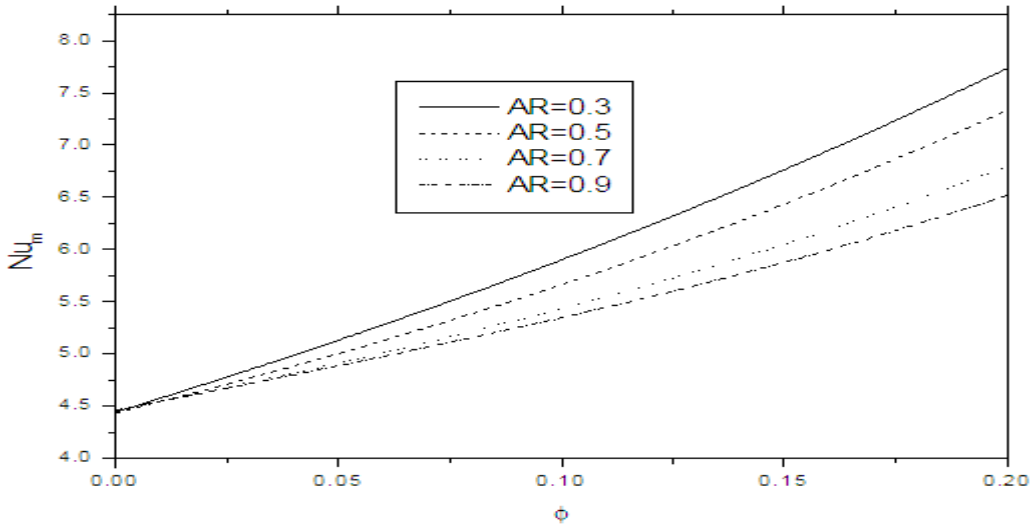

Fig.12. Variation of average Nusselt number with solid volume fraction at various aspect ratios (Cu-Water, D=0.5, Ra=10^5 and B=1/3.).

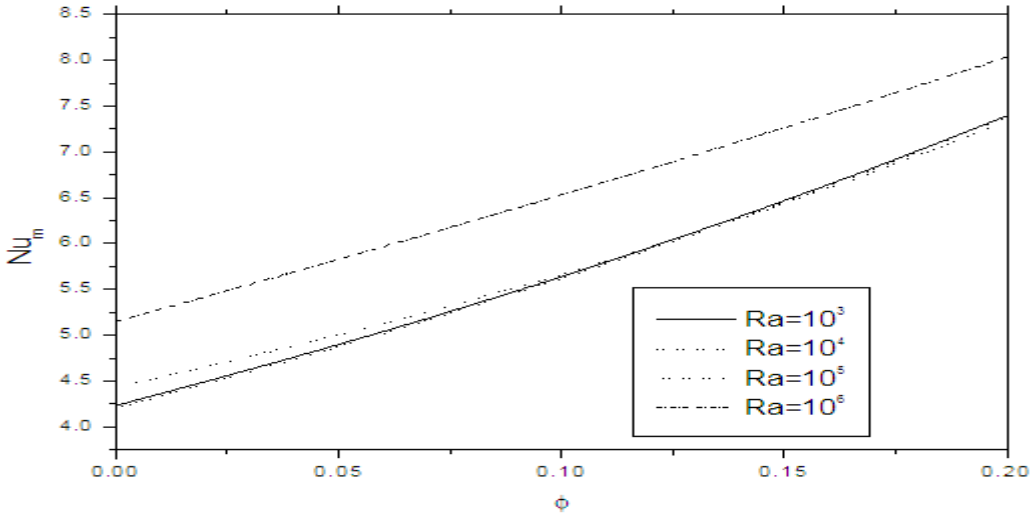

Fig.13. Variation of average Nusselt number with solid volume fraction at various Rayleigh numbers (Cu-Water, D=0.5, AR=0.5 and B=1/3.).

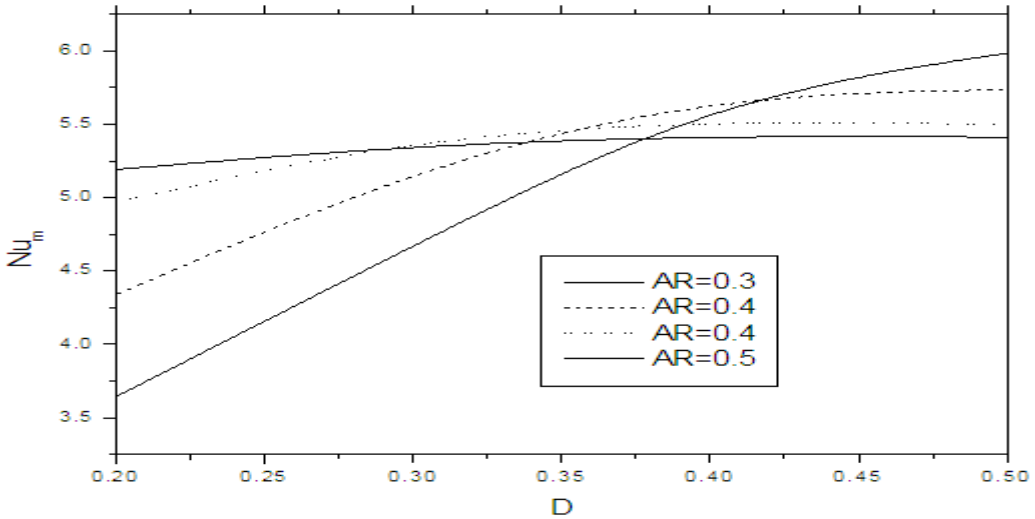

Fig.14. Variation of average Nusselt number with heat source location at various aspect ratios (Cu-Water, B=1/3., B=1/3,Ra=10^5 and ϕ=0.1).

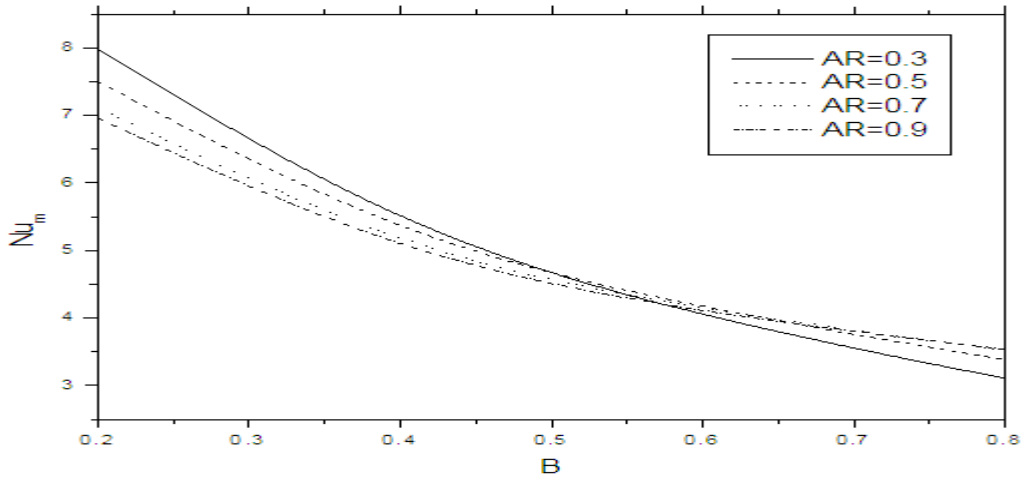

Fig.15. Variation of average Nusselt number with heat source length at various aspect ratios (Cu-Water, B=1/3., B=1/3,Ra=10^5 and ϕ=0.1).

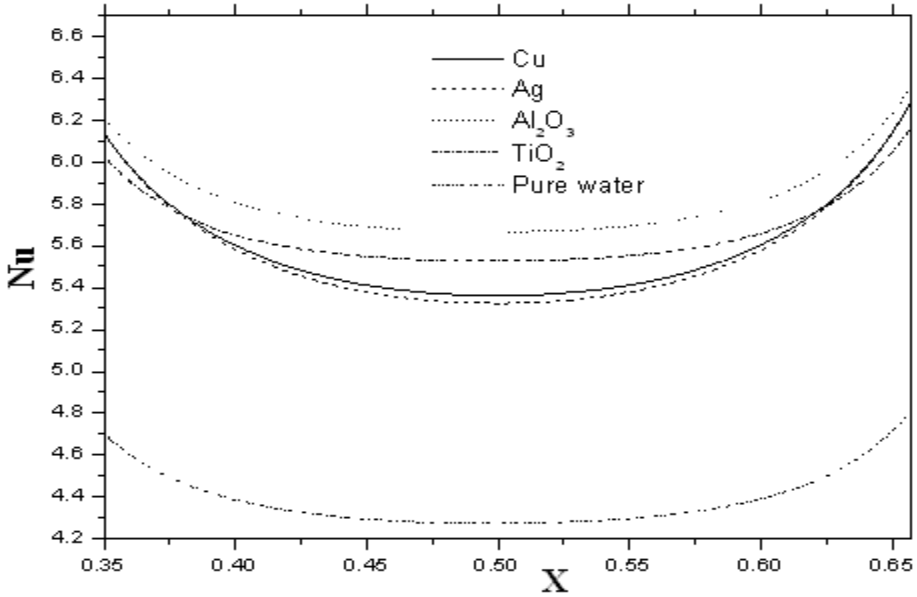

Fig.16. Variation of local Nusselt number along the heat source at the top for different types of nanofluid (D=0.5, B=1/3,Ra=10^5 and AR=0.5).

Table 1. Thermo-physical properties of water and nanoparticles.

	Pure water	Copper(Cu)	Silver (Ag)	Alumina Al_2O_3	Titanium Oxide (TiO_2)
$\rho(kgm^{-3})$	997.1	8933	10500	3970	4250
$C_p(Jkg^{-1}K^{-1})$	4179	385	235	765	686.2
$k(Wm^{-1}K^{-1})$	0.613	401	429	40	8.9538
$\beta(K^{-1})$	21×10^{-5}	1.67×10^{-5}	1.89×10^{-5}	0.85×10^{-5}	0.9×10^{-5}

Table 2. Comparison of ψ_{max} and θ_{max} .

Ra	Haajizadeh et al.[32]		Grosan et al.[27]		Present Work	
	ψ_{max}	θ_{max}	ψ_{max}	θ_{max}	ψ_{max}	θ_{max}
10	0.078	0.130	0.079	0.127	0.0799	0.1272
10^3	4.880	0.118	4.833	0.116	4.8266	0.117

Table 3. Grid independency results

	Nu_m	θ_{max}	ψ_{max}
36x36	3.413	0.990	0.587
66x66	4.757	0.973	7.725
96x96	4.684	0.990	6.024
126x126	5.241	0.983	10.676

Table 4.Results for the base case (φ=0.1, AR=0.3, B=1/3., D=.5).

Ra	nanotypes	Nu_m	θ_{max}	ψ_{max}
10^3	Cu	5.639	0.194	0.01
	Ag	5.640	0.194	0.01
	AL_2O_3	5.572	0.196	0.027
	TiO_2	5.3633	0.204	0.03
10^4	Cu	5.6179	0.194	0.099
	Ag	5.6211	0.194	0.093
	AL_2O_3	5.5359	0.195	0.241
	TiO_2	5.3272	0.202	0.266
10^5	Cu	5.6599	0.187	0.691
	Ag	5.6385	0.188	0.681
	AL_2O_3	5.8706	0.177	1.166
	TiO_2	5.7126	0.181	1.203
10^6	Cu	6.5310	0.157	1.897
	Ag	6.4705	0.158	1.968
	AL_2O_3	6.8025	0.150	2.548
	TiO_2	6.5903	0.155	2.582

Table 5.Results for the base case (φ=0.1, AR=0.3, Ra=10^5, D=.5).

AR	nanotypes	Nu_m	θ_{max}	ψ_{max}
0.3	Cu	5.898	0.17982	0.19475
	Ag	5.899	0.18011	0.18820
	AL_2O_3	5.856	0.17869	0.37906
	TiO_2	5.646	0.18489	0.40310
0.5	Cu	5.66	0.18653	0.69135
	Ag	5.638	0.18784	0.68099
	AL_2O_3	5.871	0.17651	1.16578
	TiO_2	5.713	0.18097	1.20345
0.7	Cu	5.43	0.19207	1.34306
	Ag	5.369	0.19474	1.35531
	AL_2O_3	5.914	0.17439	1.97483
	TiO_2	5.792	0.17787	2.00221
0.9	Cu	5.345	0.19429	1.94181
	Ag	5.263	0.19756	1.98595
	AL_2O_3	5.927	0.17418	2.66769
	TiO_2	5.812	0.17750	2.68667